Analytical and Bioanalytical Chemistry
https://doi.org/10.1007/s00216-022-03923-w

RESEARCH PAPER

Ultrasensitive detection of plant hormone abscisic acid-based surface-enhanced Raman spectroscopy aptamer sensor

Yanyan Zhang[1,2] · Linze Li[1,2] · Hao Zhang[1,2] · Junjian Shang[1,2] · Can Li[1,2] · Syed Muhammad Zaigham Abbas Naqvi[1,2] · Zephania Birech[3] · Jiandong Hu[1,2,4]

Received: 19 October 2021 / Revised: 9 January 2022 / Accepted: 24 January 2022

Abstract

Abscisic acid (ABA), as the most common plant hormone in the growth of wheat, can greatly affect the yield when its levels deviate from normal. Therefore, highly sensitive and selective detection of this hormone is greatly needed. In this work, we developed an aptamer sensor based on surface-enhanced Raman spectroscopy (SERS) and applied it for the high sensitivity detection of ABA. Biotin-modified ABA aptamer complement chains were modified on ferrosoferric oxide magnetic nanoparticles (Fe_3O_4MNPs) and acted as capture probes, and sulfhydryl aptamer (SH-Apt)-modified silver-coated gold nanospheres (Au@Ag NPs) were used as signal probes. Through the recognition of the ABA aptamer and its complementary chains, an aptamer sensor based on SERS was constructed. As SERS internal standard molecules of 4-mercaptobenzoic acid (4-MBA) were encapsulated between the gold core and silver shell of the signal probes; the constructed aptamer sensor generated a strong SERS signal of 4-MBA after magnetic separation. When there were ABA molecules in the detection system, with the preferential binding of ABA aptamer and ABA molecule, the signal probes were released from the capture probes, after magnetic separation, leading to a linear decrease in SERS intensity of 4-MBA. Thus, the detection response was linear over a logarithmic concentration range, with an ultra-low detection limit of 0.67 fM. In addition, the practical use of this assay method was demonstrated in ABA detection from fresh wheat leaves, with a relative error (RE) of 5.43–8.94% when compared with results from enzyme-linked immunosorbent assay (ELISA). The low RE value proves that the aptamer sensor will be a promising method for ABA detection.

Keywords Abscisic acid · Aptamer sensor · Surface-enhanced Raman spectroscopy (SERS) · Wheat leaves · Signal probes · Capture probes

Introduction

Abscisic acid (ABA), an endogenous hormone of wheat, is an organic signal molecule produced by wheat growth and development metabolism [1]. The content of ABA in wheat is very low, only 0.038–13.2 nM [2], and varies with different stages and parts of wheat growth [3]. However, ABA has significant physiological effects on wheat growth [4] and plays a crucial role in wheat growth, development, and environmental response [5]. The change in ABA content in different growth stages is directly related to the vigor, lodging resistance, photosynthetic performance, and drought resistance of wheat seeds [6, 7]. Therefore, quantitative detection or real-time monitoring of ABA concentrations in wheat at different development stages can, on the one hand, monitor the growth and development of wheat, enabling timely intervention against the influence of the harsh environment on wheat growth. On the other hand, it is of fundamental significance to further understand the molecular mechanism of plant hormones. In order to quickly quantify or detect ABA content in plants at different growth stages, it is very important to develop sensitive ABA detection methods. At present, various analytical techniques have been

✉ Jiandong Hu
jdhu@henau.edu.cn

1 College of Mechanical and Electrical Engineering, Henan Agricultural University, Zhengzhou 450002, China

2 Henan International Joint Laboratory of Laser Technology in Agricultural Sciences, Zhengzhou 450002, China

3 Department of Physics, University of Nairobi, Nairobi 30197, Kenya

4 State Key Laboratory of Wheat and Maize Crop Science, Zhengzhou 45002, China

Published online: 10 February 2022

used to detect ABA, such as colorimetry [8], local surface plasmon resonance (LSPR) [9], chromatography [10], and electrochemical methods [11], among others [12]. Although these methods have sufficient accuracy, they also have the disadvantages of large sample demand, cumbersome pretreatment caused by high reagent consumption, high requirements for professional operators, and high detection costs [13]. Therefore, it is necessary to develop a microassay with high sensitivity, lower detection limit, less sample consumption, and fewer sample pretreatment steps for ABA detection in plant samples.

Raman spectroscopy is the inelastic scattering spectroscopy of molecules, which can reflect the internal harmonic vibration frequency and the vibration energy levels of molecules [14]. Surface-enhanced Raman spectroscopy (SERS) combines molecular vibrational Raman scattering with the plasma of noble metal nanomaterials, which greatly enhances the intensity and application of Raman spectroscopy [15]. In recent years, with the development of laser and sensor technology, SERS has been widely used in new material analysis [16], cultural relic identification [17], national defense security [18], and food safety inspection [19]. Despite the success of recent applications, quantitative SERS is still faced with challenges, which is essentially due to the fluctuation of SERS hot spots [20]. Gold and silver nanomaterials are common SERS substrate materials; gold has better stability, and the enhancement of silver is stronger [21]. Thus, we can use the properties of gold, silver or their hybrid to to enable the enhancement of the molecular signals [22]. In order to solve the quantitative problem of SERS, in addition to improving the structural uniformity of gold or silver or their hybrid substrates, an internal standard method has received extensive attention as an effective strategy [23]. In this method, SERS signals of internal standard molecules embedded between core–shell nanostructures were used to calibrate the sample signals [24]. For example, Dai et al. prepared Au@Ag core–shell nanoparticles labeled with 4-mercaptopyridine (Mpy) as a SERS substrate for successful quantitative detection of the living cells in the human body [25]. In addition, Lin et al. encapsulated an internal standard 4-mercaptobenzoic acid (4-MBA) in core–shell nanoparticle as SERS enhanced substrate for the quantitative detection of pesticide residues on vegetable surfaces [26]. In conclusion, core–shell nanoparticles embedded with internal standard molecules have been shown to be an effective method to improve the accuracy of SERS detection.

Compared with the expensive antibody-antigen binding analysis, aptamer has the advantages of low acquisition cost [27], strong binding affinity with the target [28], and more stable performance, and has been widely used in the field of biosensors [29]. In recent years, more and more aptamers were combined with SERS technology to form a new type of sensor for virus, DNA, and biomarker detection [30]. For instance, Man et al. constructed a multifunctional biological molecular detection platform combining the schizotypal aptamer with photo-induced enhanced Raman spectroscopy for ultrasensitive detection of adenosine triphosphate, cocaine, and thrombin [31]. In previous research, Hu et al. optimized ABA aptamer from the literature [32], utilized the optimized ABA aptamer to build LSPR biosensor for ABA detection, and achieved good results. This demonstrated that the optimized aptamer to the target ABA has stronger binding affinity and specificity, more suitable for the capture of the target molecules [9]. Furthermore, ferrosoferric oxide magnetic nanoparticles (Fe_3O_4MNPs) have the ability for rapid separation and signal enrichment, and they can reduce and weaken the influence of impurity molecules on the target molecular signal, which is useful for obtaining strong SERS intensity [33]. Therefore, Fe_3O_4MNPs have attracted increasing attention in the field of SERS analysis [34]. However, as far as we know, there is no report on the combination of Fe_3O_4MNPs and Au@Ag core–shell nanoparticles as an ABA aptamer sensor. Therefore, combining Fe_3O_4MNPs with Au@Ag core–shell nanoparticles to develop a SERS aptamer sensor for ABA detection is of great significance.

In this work, a novel SERS aptamer sensor based on Fe_3O_4MNPs combined with Au@Ag Nps was employed in ABA detection. Firstly, streptavidin-modified Fe_3O_4MNPs and Au@Ag Nps were prepared. The internal standard molecules 4-MBA were embedded between the gold core and silver shell in advance to stabilize the SERS signal and prevent interference from the external matrix. The role of Fe_3O_4MNPs is to facilitate enrichment and separation and provide binding sites for aptamers. Next, the biotin-modified complementary chain cDNA6 was combined with Fe_3O_4MNPs as the capture probes and ABA aptamer terminal with sulfhydryl group (SH-Apt)-modified Au@Ag NPs by Ag-S covalent bond was used as the signal probes. By specifically recognizing between cDNA6 and ABA aptamer, the SERS aptamer sensor was constructed by DNA identification and hybridization of capture probes and signal probes, which produced the highest SERS signals of 4-MBA after magnetic separation. Finally, in the presence of ABA molecules, the aptamers on Au@Ag Nps preferentially and selectively bound to ABA molecules, leading to the release of signal probes from capture probes, causing a decrease in SERS intensity of 4-MBA after magnetic separation. The ABA level in the sample could be quantified by the inverse relationship between ABA concentration and SERS intensity of 4-MBA. The aptamer sensor developed by this method showed good sensitivity and selectivity in ABA detection. In addition, the magnetic separation of Fe_3O_4MNPs greatly simplifies the detection process. Therefore, the proposed SERS aptamer sensor can be used as a new tool for plant hormone detection to meet the trace detection needs and

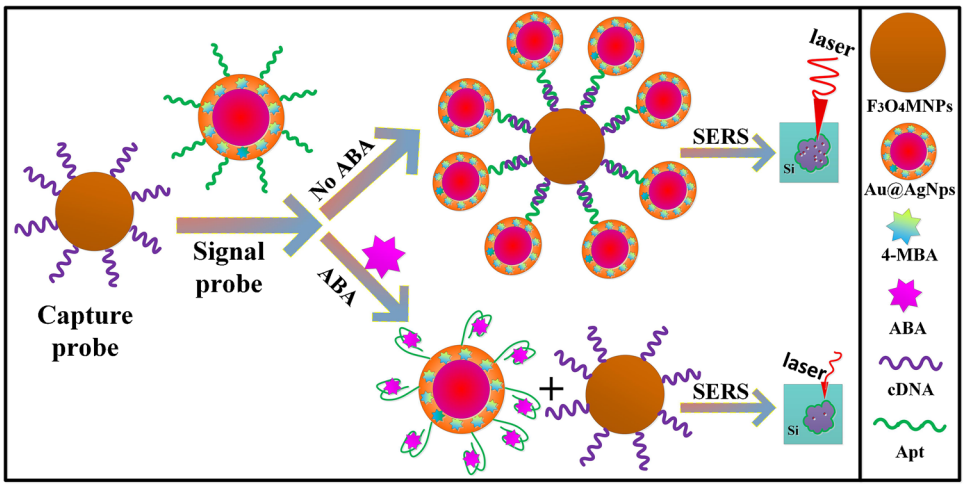

Scheme 1 The detection schematic diagram for ABA detection use the SERS aptamer sensor

further to guarantee the progress of agricultural engineering (Scheme 1).

Experimental section

Materials

Chloroauric acid hydrate ($AuCl_3{\cdot}HCl{\cdot}4H_2O$), Silver nitrate ($AgNO_3$), and L-ascorbic acid (AA) were purchased from Aladdin Reagent Co., Ltd. (Shanghai, China). ABA powder, gibberellin A3 (GA3), indole-3-acetic acid (IAA), cytokinin (CTK), rhodamine 6G (R6G, $C_{28}H_{30}N_2O_3$), 4-mercaptobenzoic acid (4-MBA), sodium citrate dihydrate ($C_6H_5Na_3O_7{\cdot}2H_2O$), polyethylene glycol sorbitan monolaurate (Tween 20) were purchased from Sigma-Aldrich (USA). Ferrosoferric oxide magnetic nanoparticles (Fe_3O_4MNPs) modified by streptavidin, sulfhydryl-terminal ABA aptamer (SH-Apt), and biotin-terminal ABA complementary aptamer were specially customized by Sangon Biotech Co., Ltd. (Shanghai, China). The sequence of DNA is shown in Electronic Supplementary Material Table S1. DNA quenching was maintained at 95 °C for 5 min followed by rapid cooling in ice water, and the quenched DNA was stored in the refrigerator. Before the experiment, all the glassware was soaked overnight in aqua regia [HCl: HNO_3 = 3:1(*v*/v)] and ultrasonically cleaned, and washed repeatedly with ultrapure water.

Instruments

The magnetism of Fe_3O_4MNPs was acquired by a BKT-4500 vibrating-sample magnetometer (Beijing Xinke High-Tech Co., Ltd). The SERS signals were collected by a confocal Raman microscopic system (Pioneer Technology Co., Ltd., Beijing, China). In the process of spectral acquisition, a 532 nm laser was used as the excitation source, a ×100 objective lens was used to focus the laser, the scanning range was 800–1800 cm^{-1} and the integral time was 5 s. The UV-vis spectra were recorded using a UV-vis spectrophotometer (Nanjing Feile Instrument Co., Ltd., Nanjing, China) with operating wavelengths of 300–700 nm. Transmission electron microscope (TEM) images were taken on a JEM-1400 Plus instrument (JEOL Ltd., Tokyo, Japan) operating at 120 kV. Zeta potentials and dynamic light scattering (DLS) distributions were obtained by a particle and molecular size analyzer (Zetasizer Nano ZS, Malvern Instruments Ltd., Melvin, UK).

Functionalization of Fe_3O_4MNPs and Au@Ag NPs with DNA

The streptavidin-modified Fe_3O_4MNPs 300 nm in size (Fig. S4a) were purchased from Sangon Biotech Co., Ltd. (Shanghai, China). The core–shell Au@Ag NPs were prepared in three steps: (1) synthesizing Au NPs; (2) modifying the internal standard molecules 4-MBA on the gold core; (3) generating a 10 nm-thick silver shell. Therefore, before the Ag shell coating, we optimized the concentration of 4-MBA to 1 mM. The optimization methods for the concentration of 4-MBA refer to the literature [35]. In order to obtain a strong and stable SERS signal, the amounts of $AgNO_3$ were optimized to obtain an optimal thickness of the Ag shell (see Electronic Supplementary Material Fig. S1). The optimization methods for the amounts of $AgNO_3$ refer to the literature [36]. Considering SERS activity and stability, we selected Au@Ag NPs with Au core diameter of about 50 nm and Ag shell thickness of about 10 nm as the best SERS substrate in our experiment for the next study.

The capture probes were prepared by coating biotin-modified cDNA6 on the streptavidin-modified Fe_3O_4MNPs. Briefly, a 20 µL solution of Fe_3O_4MNPs at a concentration of 50 mg/mL^{-1} was washed three times with ultrapure water, then diluted and suspended in PBS to a final concentration

of 2.5 mg/mL^{-1}. Then, 6 µL of 100 µM cDNA6 solution was injected into the Fe_3O_4MNPs. The resulting solution was gently shaken at room temperature for 30 min using a thermostatic oscillator. After magnetic separation, the excess cDNA6 chain was removed with ultrapure water. Finally, the obtained capture probe was dispersed in ultrapure water, and the final concentration was 1 mg/mL^{-1}.

Signal probes were prepared by coating the ABA aptamer on the core–shell Au@Ag NPs. The activated SH-Apt of 100 µM 3 µL was added to 3 mL Au@Ag NPs and incubated at room temperature (25 °C) for 12 h. Next, unbound aptamers were removed by centrifugation at 10,000 rpm for 10 min, and the sediment was dispersed in ultrapure water for further use.

Construction of SERS aptamer sensor for abscisic acid quantitative detection

The SERS aptamer sensor was produced (Au@Ag@Apt-Fe_3O_4MNPs@cDNA6) by mixing capture probes (Fe_3O_4MNPs@cDNA6) and signal probes (Au@Ag@Apt) in different volume ratios and hybridizing for 1 h at 37 °C. The resulting sensor solution was cleaned with ultrapure water and separated with a magnet. The precipitate was dispersed in ultrapure water and stored at 4 °C for later use.

For ABA detection, 50 µL aliquots of different concentrations (1×10^{-15} M, 1×10^{-14} M, 1×10^{-13} M, 1×10^{-12} M, 1×10^{-11} M, 1×10^{-10} M, 1×10^{-9} M, 1×10^{-8} M) of ABA were incubated with the 50 µL SERS aptamer sensor for 40 min at 37 °C with gentle shaking by a thermostatic oscillator (SHA-C, Aohua Instrument Co., Changzhou, China). After magnetic separation, the obtained mixture was washed with ultrapure water under manual shaking and resuspended in 100 µL ultrapure water. Then, 5 µL of the mixture was dropped on the silicon wafer and then dried naturally in the air for testing. The limit of detection (LOD) of ABA was calculated using the equation $3S_b/b$, where S_b is the standard deviation of the intensity of the blank sample at 1589 cm^{-1} Raman shift, and b is the slope of the drawn standard curve [37].

Selectivity evaluation

Due to the complexity of the action of plant hormones on plant growth mechanisms, various endogenous hormones restrict and complement each other. Other endogenous hormones such as gibberellin A3 (GA3), indole-3-acetic acid (IAA), and cytokinin (CTA) may disturb the detection of abscisic acid. In order to investigate the selectivity of the proposed aptamer SERS sensor, gibberellin A_3 (GA_3), indole-3-acetic acid (IAA), and cytokinin (CTA) at a concentration of 1 mM were used in the assay instead of ABA.

Real sample analysis

Measuring the detection ability in real samples is an important indicator to judge the practical utility of the sensor. Therefore, in order to verify the feasibility of the aptamer sensor in detecting ABA in real samples, we selected mature wheat leaves to prepare real samples, and the extraction method for real samples referred to [38]. The concentration of the real samples was determined by both enzyme-linked immunosorbent assay (ELISA) and SERS methods.

Results and discussion

Morphological and LSPR characterization of the NPs

The Au and the Au@Ag NPs were fairly spherical in shape, with the latter surrounded by a 10 nm Ag shell as displayed in the TEM images of Fig. 1a and b. The silver shell thickness was optimized by reducing different doses of $AgNO_3$ with AA: the thicker the silver shell, the higher the SERS enhancement. However, the silver shell with a thickness of more than 10 nm will block the laser irradiation and reduce the SERS intensity of internal standard molecules. Therefore, a thickness of 10 nm was used as the thickness of the silver shell of the core–shell nanoparticles in this study. The optimization process of silver shell thickness was shown in Electronic Supplementary Material Fig. S1. The sizes of Au NPs, Au@Ag NPs, and Au@Ag@Apt NPs were 50, 60, and 63 nm in diameter respectively as confirmed by the dynamic light scattering (Fig. 1c). A LSPR band for both Au@Ag NPs and Au@Ag@Apt NPs was observed centered around a wavelength of 420 nm but with diminished absorbance for the latter and a slight change in the color of the solution (darkened), as seen in Fig. 1d. The zeta potential of Au@Ag NPs was found to be −40.7 mV, and this was due to the reduction of silver nitrate by trisodium citrate, and the citrate is negatively charged. After the conjugation of SH-Apt onto Au@Ag NPs, the surface potential increased to −24.5 mV. These changes in electric potential (see Electronic Supplementary Material Fig. S2), absorbance (Fig. 1d), and hydrodynamic particle size (Fig. 1c) indicated that aptamers were successfully modified onto the surfaces of the Au@Ag NPs.

The successful assembly of the complementary aptamer cDNA6 on the streptavidin-modified Fe_3O_4MNPs was also assessed by zeta potential measurement (Fig. 2b). The zeta potential of Fe_3O_4MNPs was 28.2 mV. After the conjugation of biotin-modified cDNA6 onto Fe_3O_4MNPs, the surface potential increased to 46.5 mV. The magnetic hysteresis loops were recorded to study the magnetism of magnetic beads and Fe_3O_4MNPs@cDNA6. The saturation magnetization (MS) value of Fe_3O_4MNPs was 38.9 emu·g^{-1} (Fig. 2a, black line), exhibiting a superparamagnetic property.

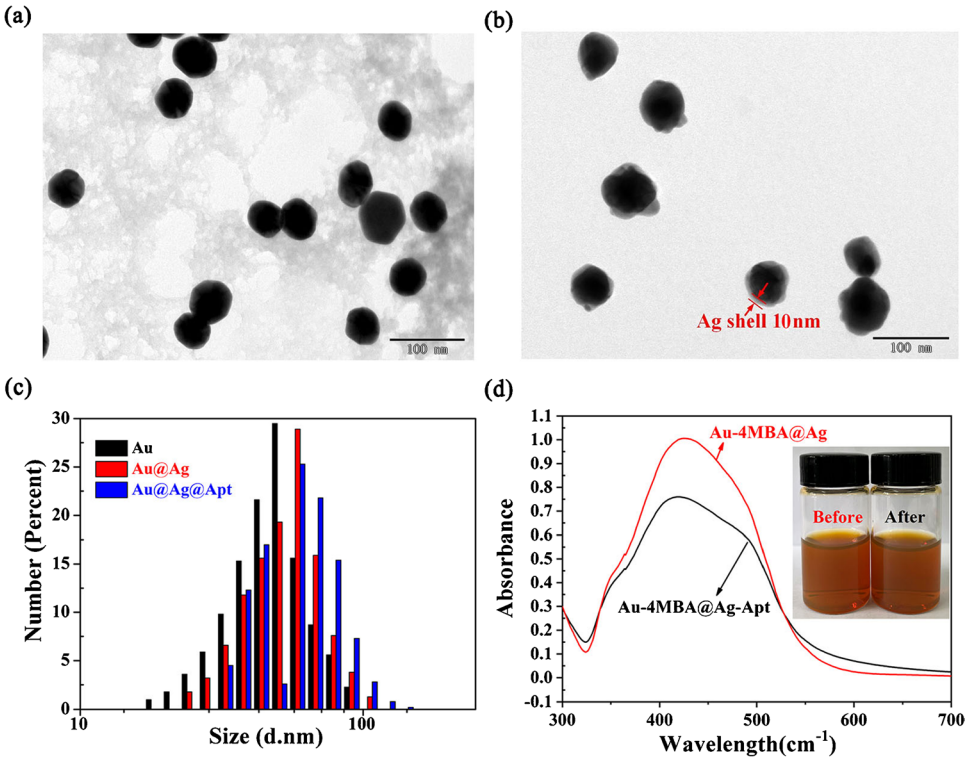

Fig. 1 Characterization of the signal probes (Au@Ag@Apt NPs). (**a**), (**b**) TEM images of Au NPs and Au@Ag NPs. (**c**) The Au Nps, Au@Ag Nps, and Au@Ag@Apt Nps are indicated with numbers, (**d**) UV–Vis spectra and color of Au@Ag NPs and Au@Ag@Apt NPs

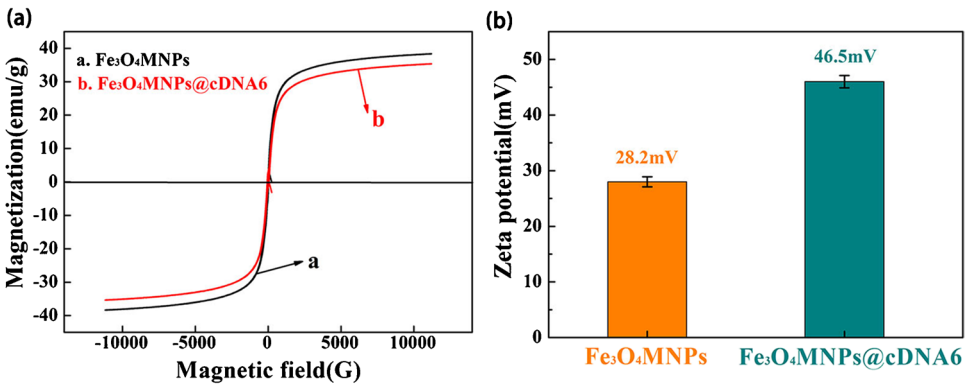

Fig. 2 Characterization of capture probes (Fe_3O_4MNPs@cDNA6). (**a**) Magnetic hysteresis curve; (**b**) zeta potential measurements

In addition, only a slight decrease in magnetization of Fe_3O_4MNPs@ cDNA6 was observed (Fig. 2a, red line) after coating with the complementary aptamer, indicating that Fe_3O_4MNPs still retained good magnetism after modification of cDNA6.

Optimization of the SERS aptamer sensor

However, some factors inevitably affect the performance of the sensor. Therefore, we investigated these potential factors. It is clear from Fig. 3a and b that the strongest SERS intensity was obtained with the binding of the Fe_3O_4MNPs@CDNA6 as capture probes to the signal probes, indicating that CDNA6 had the strongest binding force with the ABA aptamer. This is consistent with the results of UV-Vis spectra (Fig. 3c and d). UV-Vis spectra showed that the absorbance of Au@Ag@Apt-Fe_3O_4MNPs@cDNA6s changed the most when the eight capture probes were combined with the signal probes, indicating that the signal probes and MB-cDNA6 had the strongest recognition ability. Due to the relatively stronger recognition affinity between the cDNA6 and the aptamer, more signal probes were bound to the capture probes after the combination of the two probes, resulting in an increase in the concentration of the signal probes in the mixed solution, and thus the absorbance. Therefore, the optimal aptamer sensor was established using the Fe_3O_4MNPs@cDNA6 as the capture probes.

It is also very important to select an appropriate ratio between capture probes and signal probes for establishing a sensitive SERS aptamer sensor. The capture probes and

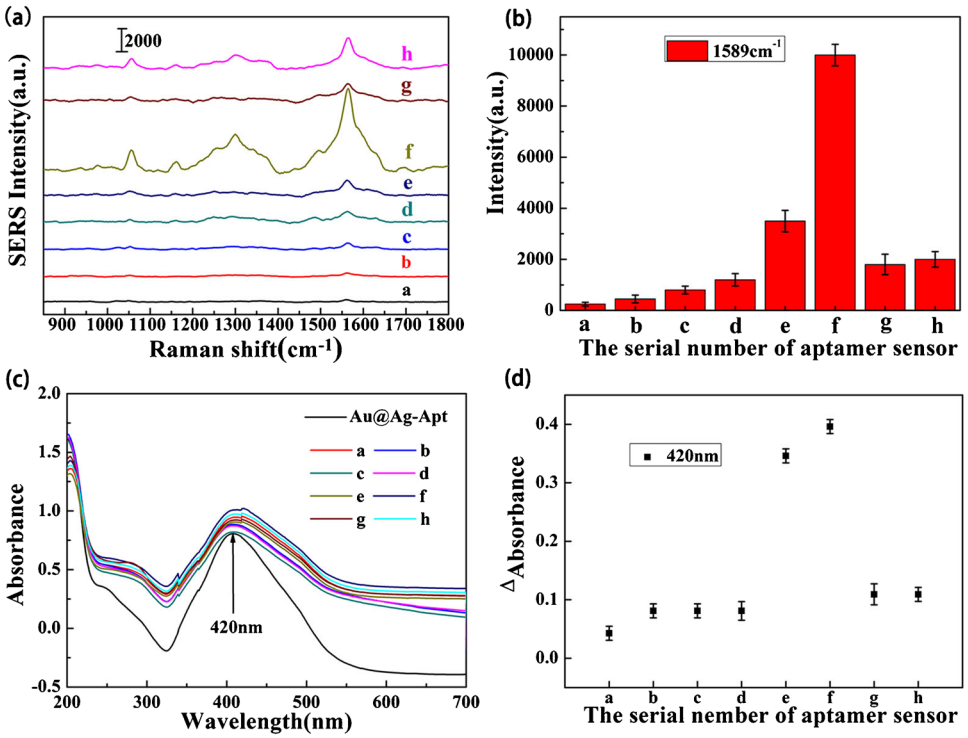

Fig. 3 Selection of aptamer supplement chain. (**a**) SERS spectral curve and (**b**) intensity histogram at 1589 cm^{-1} of eight kinds of capture probes mixed with signal probes. (**c**) Absorbance curve and (**d**) absorbance changes in signal probe combined with eight kinds of capture probe. The letters a, b, c, d, e, f, g, and h in the figure (**a**)-(**d**) respectively represent Au@Ag@Apt-Fe_3O_4MNPs@cDNA1, Au@Ag@Apt-Fe_3O_4MNPs@cDNA2, and so on up to Au@Ag@Apt-Fe_3O_4MNPs@cDNA8

signal probes with different volume ratios (1:1, 1:1.25, 1:1.5, 1:1.75, 1:2, 1:2.25, 1:2.5) were incubated at 37 °C until the signal probes and the capture probe were fully integrated. After the mixture was centrifuged, collected, and dispersed, the SERS detection was performed. As illustrated in Fig. 4a and Electronic Supplementary Material Fig. S3, when the volume ratio of the capture probes to the signal probes was 1:2.5, the strongest SERS intensity was obtained. However, when the volume ratio reached 1:2, if the volume of the signal probes continued to increase, the SERS signal changed very little. This indicates that when the volume ratio was 1:2, the signal probes completely covered the capture probes. Therefore, the optimal aptamer sensor was built based on the ratio of 1:2 for capture probes over signal probes. In order to further verify the successful construction of the SERS aptamer sensor based on signal probes, TEM images were obtained. TEM images of the capture probes and signal probes are shown in Electronic Supplementary Material Fig. S4a and b, respectively. Figure S4c shows that the signal probes (Au@Ag@apt NPs) and the capture probe (Fe_3O_4MNPs@cDNA6) were uniformly bonded by DNA hybridization, which is consistent with the literature [39, 40].

Furthermore, because the ABA aptamer preferentially combined with ABA, leading to the capture probes releasing signal probes, the SERS intensity of the internal standard molecule 4-MBA decreased. Therefore, by optimizing the competitive reaction time of ABA and aptamer, accurate results were be obtained. As can be seen from Fig. 4b, the SERS intensity of 4-MBA gradually weakened with the increase in competitive reaction time, but when the reaction time reached 40 min, SERS intensity no longer weakened

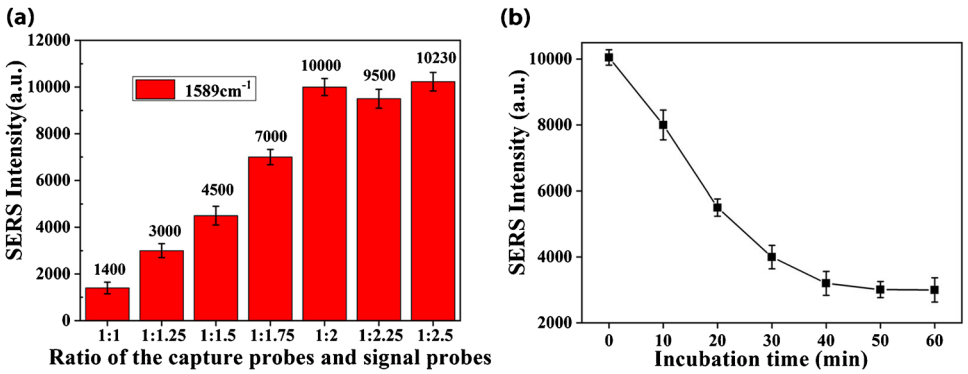

Fig. 4 SERS intensity of 4-MBA at 1589 cm^{-1} of (**a**) different volume ratios (1:1, 1:1.25, 1:1.5, 1:1.75, 1:2, 1:2.25, 1:2.5) of capture probes and signal probes and (**b**) different incubation times (10, 20, 30, 40,50, 60 min) of ABA (1×10^{-8} M)

and reached a platform, so 40 min was chosen as the competitive reaction time.

The detection of abscisic acid-based aptamer sensor

The Raman characteristic peaks of ABA powder are shown in Electronic Supplementary Material Fig. S5. The strongest Raman peak shift at 1637 cm^{-1} was derived from the stretching vibration of the C=C double bond in the ABA molecular structure. The attribution of other characteristic peaks and the molecular structure of ABA are shown in Electronic Supplementary Material Table S2. In fact, in the process of ABA detection, there was no obvious characteristic peak of ABA in the detection spectrum, because the introduction of ABA led to the separation of the signal probes and the capture probes, and the SERS intensity of the 4-MBA on the capture probes decreased, so the relationship between ABA concentration and SERS intensity of the 4-MBA molecule was established.

Based on the constructed SERS aptamer sensor, the changes in SERS intensity of the 4-MBA molecules caused by different concentrations of ABA were detected. As can be seen from Fig. 5a, within the range of 1×10^{-15} M to 1×10^{-8} M, SERS intensity gradually decreased with the increase in ABA concentration, which was because the increase in ABA concentration led to the increased release of signal probes. The obvious Raman peak of internal standard 4-MBA at 1589 cm^{-1} was selected to establish a linear relationship, as shown in Fig. 5b. There was a strong linear relationship between the SERS intensity at 1589 cm^{-1} and logarithmic ABA concentrations from 1×10^{-15} M to 1×10^{-8} M. According to Fig. 5b, the linear regression equation was $y=-1172x+7484$, with a correlation coefficient R^2 of 0.9875, and the calculated limit of detection (LOD) of ABA was 0.67 fM. In addition, compared with other ABA assays reported previously (Table 1), the SERS aptamer sensor had a wider linear range and lower LOD for ABA detection; the LOD was five orders of magnitude lower than that for chromatographic detection of ABA, and the detection time was shorter. Once the signal probe-based SERS aptamer sensor was set up, the testing only took a few seconds.

Specificity evaluation

Some wheat endogenous hormones were introduced to test the selectivity of the aptamer SERS sensor for ABA. As shown in Fig. 6, in the presence of the GA_3, IAA, or CTK, no obvious change was observed in the SERS signal. On the contrary, the concentration of ABA was 10,000 times lower than other endogenous hormones in wheat, but led to an obvious decrease in SERS signal intensity. These results demonstrate that the developed aptamer sensor has good selectivity for ABA.

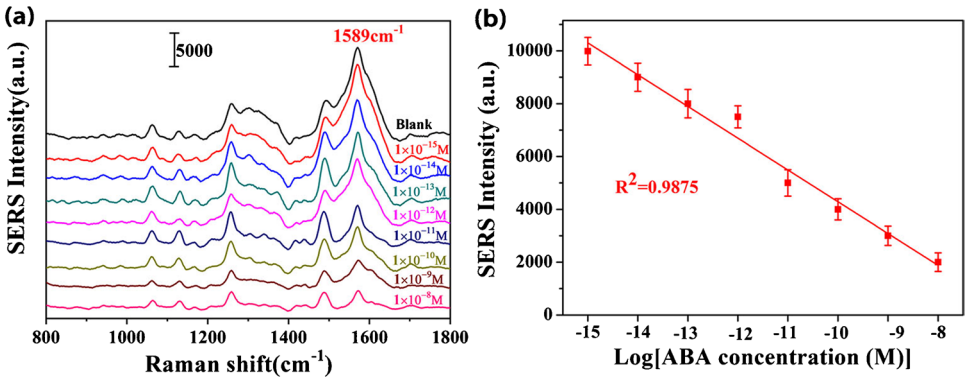

Fig. 5 (**a**) SERS spectra and (**b**) calibration curve of the signal probe-based aptamer sensor for abscisic acid at different concentrations (1×10^{-15} M, 1×10^{-14} M, 1×10^{-13} M, 1×10^{-12} M, 1×10^{-11} M, 1×10^{-10} M, 1×10^{-9} M, 1×10^{-8} M, from top to bottom). Error bars show the standard deviation of three repeated experiments

Table 1 Comparison of the results for the developed method with those of existing methods for abscisic acid detection

Number	Method	Detection range	LOD	References
1	Capillary electrophoresis	0.1–10 μM	0.28 nM	[41]
2	Electrochemical immunoassay	10 ng/mL–10 μg/mL	5 ng/mL	[11]
3	Chemiluminescence	1pM–10 nM	1pM	[12]
4	Chromatography	0.01 ng/mL–0.74 μg/mL	0.01 ng/mL	[10]
5	Colorimetric	5 nM–10 μM	2.2 nM	[8]
6	LSPR	0.1 nM–1 mM	0.51 nM	[9]
7	SERS aptamer sensor	1fM–10 nM	0.67 fM	**This work**

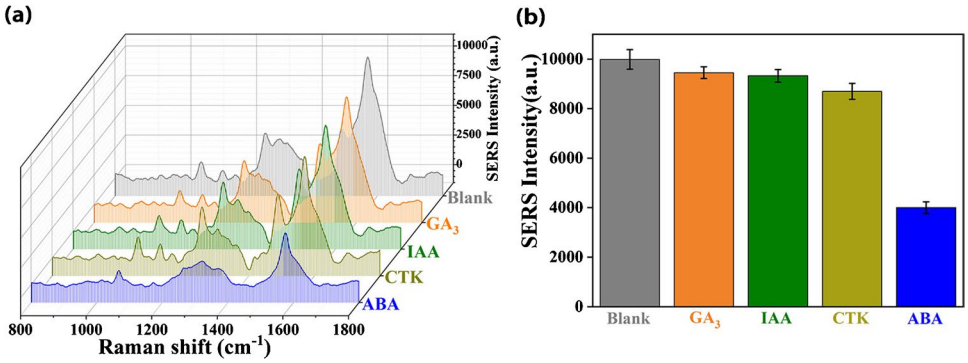

Fig. 6 Selectivity of the developed abscisic acid aptamer sensor for abscisic acid (0.1 nM) to other plant hormones (1 mM). (**a**) SERS spectra curves for blank and other wheat endogenous hormone samples. (**b**) Comparison of the relative Raman peak intensities at 1589 cm^{-1}. Error bars show the standard deviation of three repeated experiments

Table 2 Comparison of results for ABA detection in wheat samples by ELISA and SERS ($n=3$)

Sample	Mean value found by present method (nM)	Mean value found by ELISA method (nM)	Relative error compared with ELISA kits (%)
1	92.34 ± 3.28	97.65 ± 1.52	5.43
2	99.58 ± 2.32	109.36 ± 1.32	8.94
3	105.84 ± 2.73	115.34 ± 1.18	8.24

Abscisic acid determination in real wheat leaves

In order to further verify the effectiveness of the SERS method proposed in this paper in practical application, fresh leaves of mature wheat were selected for the experiment. The content of ABA in real samples was also determined by ELISA. The comparison results are summarized in Table 2. Compared with ELISA, the maximum relative error was 8.94%, and the agreement between the two methods was acceptable. The comparison results show that this method provides a feasible assay for the detection of gibberellin, indole acetic acid, and other plant hormones.

Conclusions

A high-performance SERS aptamer sensor was successfully developed by combining the multifunctional capture probes (Fe_3O_4MNPs@cDNA6) with the strong SERS intensity of the signal probes (Au@Ag@Apt). Different ABA concentrations in the sensor system caused different SERS intensity of 4-MBA molecules, which was used for the ultrasensitive detection of ABA. The linear range of ABA detection was 1 fM to 10 nM, R^2 was 0.9875, and the detection limit was 0.67 fM. The application of this method in the determination of ABA in fresh wheat leaves showed that the relative error was 5.43–8.94% compared with ELISA. Therefore, this new SERS aptamer sensor could be used as a promising analytical tool for the detection of ABA in practical samples. These satisfactory results indicate that the new method developed in this study based on SERS is helpful for sensitive and accurate detection of ABA in plants. This new method can also be used for the analysis of other endogenous hormones in plants and animals.

Supplementary Information The online version contains supplementary material available at https://doi.org/10.1007/s00216-022-03923-w.

Funding The authors are thankful to the National Natural Science Foundation of China (grant numbers 32071890, 31671581) and Agricultural Biological resources Engineering technology Foreign Scientist Workshop project of Henan province (GZS2021007).

Declarations

Competing interests The authors declare that they have no known competing financial interests or personal relationships that could have appeared to influence the work reported in this paper.

References

1. Silveira V, Santa-Catarina C, Balbuena TS, Moraes FMS, Ricart CAO, Sousa MV, Guerra MP, Handro W, Floho EIS. Endogenous abscisic acid and protein contents during seed development of Araucaria angustifolia. Biol Plant. 2008;52(1):101–4.
2. Shibata M, Coelho CMM, de Garighan JA, dos Santos HP, Araldi CG, Maraschin M. Seed development of Araucaria angustifolia: plant hormones and germinability in 2 years of seeds production. New Forest. 2021;52(5):759–75.
3. Sirko A, Wawrzynska A, Brzywczy J, Sienko M. Control of ABA signaling and crosstalk with other hormones by the selective degradation of pathway components. Int J Mol Sci. 2021;22(9):4638.
4. De Y, Shi FL, Gao FQ, Mu HB, Yan WH. Siberian Wildrye (Elymus sibiricus L.) abscisic acid-insensitive 5 gene is

involved in abscisic acid-dependent salt response. Plant Basel. 2021;10(7):1351.
5. Zhu YC, Wang QY, Gao ZW, Wang Y, Liu YJ, Ma ZP, Chen YW, Zhang YC, Yan F, Li JW. Analysis of Phytohormone signal transduction in Sophora alopecuroides under salt stress. Int J Mol Sci. 2021;22(14):7313.
6. McAdam SAM, Sussmilch FC. The evolving role of abscisic acid in cell function and plant development over geological time. Semin Cell Dev Biol. 2021;109:39–45 SI.
7. Yang JF, Chen MX, Zhang JH, Hao GF, Yang GF. Structural dynamics and determinants of abscisic acid-receptor binding preference in different aggregation states. J Exp Bot. 2021;72(13):5051–65.
8. Zhou GH, Luo YZ, Xu QF, Ji XH, He ZK. Peptide-capped gold nanoparticle for colorimetric immunoassay of conjugated abscisic acid. ACS Appl Mater Interfaces. 2012;4(9):5010–5.
9. Wang S, Zhang H, Zephania B, Li DX, Li SX, Wang L, Shang JJ, Hu JD. A multi-channel localized surface plasmon resonance system for absorptiometric determination of abscisic acid by using gold nanoparticles functionalized with a polyadenine-tailed aptamer. Microchim Acta. 2020;187(1):20.
10. Yan SJ, Guo LW, Wu CE, Liang LY, Wang JD, Zhang LN. Simultaneous determination of three kinds of endogenous hormones content in seeds of post-harvest Yali pear by high performance liquid chromatography. Chin J Anal Chem. 2010;38(6):843–7.
11. Qi BB, Wu C, Liang HL, Cui KH, Fahad S, Wang ML, Liu BY, Nie LX, Huang JL, Tang H. Optimized high-performance liquid chromatography method for determining nine Cytokinins, Indole-3-acetic acid and abscisic acid. Sustainability. 2021;13(13):6998.
12. Zhou GH, Wang P, Yuan J, Qiu T, He ZK. Immunomagnetic assay combined with CdSe/ZnS amplification of chemiluminescence for the detection of abscisic acid. Sci China Che. 2011;54(8):1298–303.
13. Fu JH, Sun XH, Wang JD, Chu JF, Yan CY. Progress in quantitative analysis of plant hormones. Chin Sci Bull. 2011;56(4–5):355–66.
14. Wang PX, Sun Y, Li X, Wang L, Xu Y, Li GL. Recent advances in metal organic frameworks based surface enhanced Raman scattering substrates: synthesis and applications. Mol. 2021;26(1):209.
15. Fleischmann MP, Hendra PJ. Raman spectra of pyridine adsorbed at a silver electrode. Chem Phys. 1974;26:163–6.
16. Chen YF, Yang J, Li ZL, Li R, Ruan WD, Zhuang ZP, Zhao B. Experimental and density functional theory study of Raman and SERS spectra of 5-amino-2-mercaptobenzimidazole. Spectrochimi Acta Part A. 2016;153:344–8.
17. Badillo-Ramirez I, Saniger JM, Popp J, Cialla-May D. SERS characterization of dopamine and in situ dopamine polymerization on silver nanoparticles. Phys Chem Chem Phys. 2021;23(21):12158–70.
18. Makam P, Shilpa R, Kandjani AE, Periasamy SR, Sabri YM, Madhu C, Bhargava SK, Govindaraju T. SERS and fluorescence-based ultrasensitive detection of mercury in water. Biosens Bioelectron. 2018;100:556–64.
19. Sheng EZ, Lu YX, Xiao Y, Li ZX, Wang HS, Dai ZH. Simultaneous and ultrasensitive detection of three pesticides using a surface-enhanced Raman scattering-based lateral flow assay test strip. Biosens Bioelectron. 2021;181:113149.
20. Fan MK, Andrade GFS, Brolo AG. A review on recent advances in the applications of surface-enhanced Raman scattering in analytical chemistry. Anal Chim Acta. 2020;1097:1–29.
21. Li JF, Zhang YJ, Ding SY, Rajapandiyan P, Tian ZQ. Core–Shell nanoparticle-enhanced Raman spectroscopy. Che Rev. 2017;117(7):5002–69.
22. Kim J, Sim K, Cha S, Oh JW, Nam JM. Single-particle analysis on Plasmonic Nanogap Systems for Quantitative SERS. J Raman Spectrosc. 2020;52(2):375–85.
23. Wang XA, Shen W, Zhou BB, Yu DY, Tang XH, Liu JH, Huang XJ. The rationality of using core-shell nanoparticles with embedded internal standards for SERS quantitative analysis based glycerol-assisted 3D hotspots platform. RSC Adv. 2021;11(33):20326–34.
24. Chen RP, Du X, Cui YJ, Zhang XY, Ge QY, Dong J, Zhao XW. Vertical flow assay for inflammatory biomarkers based on Nanofluidic Channel Array and SERS Nanotags. Small. 2020;16(32):2002801.
25. Dai X, Song ZL, Song WJ, Zhang JL, Fan GC, Wang W, Luo XL. Shell-switchable SERS blocking strategy for reliable signal-on SERS sensing in living cells: detecting an external target without affecting the internal Raman molecule. Anal Chem. 2020;92(16):11496–75.
26. Lin S, Lin X, Han S, Liu YL, Hasi W, Wang L. Flexible fabrication of a paper-fluidic SERS sensor coated with a monolayer of core-shell nanospheres for reliable quantitative SERS measurements. Anal Chim Acta. 2020;1108:167–76.
27. Song MY, Khan IM, Wang ZP. Research Progress of optical Aptasensors based on AuNPs in food safety. Food Anal Methods. 2021;14(10):12161.
28. Ma XY, Lin XC, Xu XM, Wang ZP. Fabrication of gold/silver nanodimer SERS probes for the simultaneous detection of salmonella typhimurium and Staphylococcus aureus. Mikrochim Acta. 2021;188(6):202.
29. Zhou ZH, Xiao R, Cheng SY, Wang S, Shi LL, Wang CW, Qi KZ, Wang SQ. A universal SERS-label immunoassay for pathogen bacteria detection based on Fe_3O_4@au-aptamer separation and antibody-protein a orientation recognition. Anal Chim Acta. 2021;1160:338421.
30. Muhammad M, Huang Q. A review of aptamer-based SERS biosensors: design strategies and applications. Talanta. 2021;277:122188.
31. Man TT, Lai W, Xiao MS, Wang XW, Chandrasekaran AR, Pei H, Li L. A versatile biomolecular detection platform based on photo-induced enhanced Raman spectroscopy. Biosens Bioelectron. 2019;147:111742.
32. Grozio A, Gonzalez VM, Millo E, Sturla L, Vigliarolo T, Bagnasco L, Guida G, D'Arrigo C, Flora AD, Salis A, Martin EM, Bellotti M, Zocchi E. Selection and characterization of single stranded DNA aptamers for the hormone abscisic acid. Nucleic Acid Thera. 2013;23(5):322–31.
33. Zhang CY, Huang LJ, Pu HB, Sun DW. Magnetic surface-enhanced Raman scattering (MagSERS) biosensors for microbial food safety: fundamentals and applications. Trends in Food Sci Tech. 2021;113:366–81.
34. Yang EL, Li D, Yin PK, Xie QY, Li Y, Lin QY, Duan YX. A novel surface-enhanced Raman scattering (SERS) strategy for ultrasensitive detection of bacteria based on three-dimensional (3D) DNA walker. Biosens Bioelectron. 2020;172:112758.
35. Ning CF, Tian YF, Zhou W, Yin BC, Ye BC. Ultrasensitive SERS detection of specific oligonucleotides based on au@AgAg bimetallic nanorods. Analyst. 2019;144(9):2929–35.
36. Wang KQ, Sun DW, Pu HB, Wei QY. Shell thickness-dependent au@ag nanoparticles aggregates for high-performance SERS applications. Talanta. 2019;195:506–5.
37. Jiang CH, Wang Y, Song W, Lu LH. Delineating the tumor margin with intraoperative surface-enhanced Raman spectroscopy. Anal Bioanal Chem. 2019;411(18):3993–4006.
38. Wang S, Li W, Chang KK, Liu J, Guo QQ, Sun HF, Jiang M, Zhang H, Chen J, Hu JD. Localized surface plasmon resonance-based abscisic acid biosensor using aptamer-functionalized gold nanoparticles. PLoS One. 2017;12(9):e0185530.

39. He DY, Wu ZZ, Cui B, Jin ZY. A novel SERS-based aptasensor for ultrasensitive sensing of microcystin-LR. Food Chem. 2018;278:197–202.
40. He HR, Da W, Pu HB, Huang LJ. Bridging Fe3O4@au nanoflowers and au@ag nanospheres with aptamer for ultrasensitive SERS detection of aflatoxin B1. Food Chem. 2020;324:126832.
41. Liu X, Ma L, Lin YW, Lu YT. Determination of abscisic acid by capillary electrophoresis with laser-induced fluorescence detection. J Chromatogr A. 2003;1021(1–2):209–13.